Research Square

Preprints are preliminary reports that have not undergone peer review.
They should not be considered conclusive, used to inform clinical practice,
or referenced by the media as validated information.

Comparative Analysis of Nonlinear State Estimators within Fractional Model Predictive Control for a Fractional Chaotic Rössler System

Devasmito Das
École Centrale de Nantes
Ina Taralova
Ina.Taralova@ls2n.fr

École Centrale de Nantes
Jean-Jacques Loiseau
École Centrale de Nantes
Tsonyo Slavov
Technical University of Sofia

Research Article

Keywords: Fractional model predictive control, Rőssler system, nonlinear state estimation, Unscented Kalman Filter, Particle Filter, chaotic systems

Posted Date: June 12th, 2026

DOI: https://doi.org/10.21203/rs.3.rs-9852572/v1

License: This work is licensed under a Creative Commons Attribution 4.0 International License.
Read Full License

Additional Declarations: No competing interests reported.

Comparative Analysis of Nonlinear State Estimators within Fractional Model Predictive Control for a Fractional Chaotic Rössler System

Abstract

This paper presents a robust state estimation and control framework for a fractional-order Rössler system using fractional model predictive control integrated with nonlinear state observers. The system dynamics are modeled using the Grünwald–Letnikov fractional derivative, which enables efficient numerical implementation while capturing inherent memory effects. The proposed framework incorporates and systematically compares three nonlinear estimation techniques: the Extended Kalman Filter, the Unscented Kalman Filter, and the Particle Filter. These observers are evaluated within the predictive control loop under partial state measurement scenarios, including the estimation of unmeasured states from limited outputs. The study considers realistic operating conditions with additive Gaussian noise and investigates estimation accuracy, robustness to disturbances, and computational cost. Quantitative performance metrics such as root mean square error and convergence behavior are used to assess the performance of each estimator. Results demonstrate that while the Extended Kalman Filter offers computational efficiency, the Unscented Kalman Filter improves estimation accuracy for strongly nonlinear dynamics, and the Particle Filter provides enhanced robustness under higher noise levels at the expense of increased computational effort. The findings highlight the trade-offs between estimation performance and computational complexity, offering practical insights for selecting suitable observers in fractional-order chaotic systems controlled via predictive strategies.

Keywords: Fractional model predictive control, Rössler system, nonlinear state estimation, Unscented Kalman Filter, Particle Filter, chaotic systems

1 Introduction

Fractional-order dynamical systems have emerged as powerful tools for modeling and understanding complex physical phenomena characterized by memory and non-local interactions [12, 14, 16]. Classical chaotic systems such as the Rössler, Chua, Lü, Chen, Duffing, Hopf, and Lorenz models exhibit significantly richer dynamics when extended to fractional orders, enabling a more accurate representation of real-world

processes [7, 4, 2, 1, 22]. In such systems, the fractional derivative order governs the influence of historical states, thereby introducing long-range temporal dependencies that fundamentally alter system stability, bifurcation structure, and chaotic behavior [14, 16, 22]. Among these, the fractional-order Rössler oscillator provides a particularly suitable benchmark due to its relatively simple structure, consisting of two linear and one nonlinear equation, while still exhibiting complex chaotic dynamics [20, 5, 6, 2].

The control and estimation of fractional chaotic systems remain challenging due to their inherent nonlinearity, sensitivity to initial conditions, and memory-dependent dynamics. Fractional Model Predictive Control (FMPC) has shown significant promise in stabilizing such systems by explicitly incorporating fractional dynamics within the prediction model [19, 3, 6, 17, 18]. At the same time, accurate state estimation is essential for effective control, especially under partial observability and measurement noise. The Extended Kalman Filter (EKF) has been widely used for nonlinear state estimation in fractional systems due to its computational efficiency and simplicity [23, 25, 10, 24, 26, 27, 8]. However, its reliance on first-order linearization may limit its performance in strongly nonlinear and chaotic regimes [11, 9].

Despite these advances, a critical gap remains in the systematic evaluation of alternative nonlinear estimation techniques within fractional-order predictive control frameworks. In particular, the Unscented Kalman Filter (UKF) and Particle Filter (PF) offer potential advantages in handling nonlinear transformations and non-Gaussian uncertainties, respectively. However, their comparative performance in the context of fractional chaotic systems, especially when integrated with FMPC, has not been thoroughly investigated [11, 25, 10, 27, 9]. Existing studies typically focus on a single specific estimator, without providing a comprehensive analysis of estimation accuracy, robustness to noise, and computational efficiency across different filtering approaches.

To address this gap, this paper proposes a unified FMPC-based control framework integrated with multiple nonlinear state estimators, including the EKF, UKF, and PF, for the fractional-order Rössler system. The system dynamics are characterized using the Grünwald–Letnikov fractional derivative, which enables efficient numerical implementation while preserving the memory characteristics of the system. Two partial measurement scenarios are considered: (i) measurement of the state z to estimate x and y, and (ii) measurement of x and y to estimate z. The proposed framework evaluates the performance of each estimator under realistic noisy measurement conditions. In the numerical simulations, additive Gaussian process and measurement noises are considered in order to provide a controlled and fair comparison between the EKF, UKF, and PF. Although the PF is more general and can also be applied to non-Gaussian uncertainty models, the Gaussian-noise setting is retained here to ensure direct comparison with the Kalman-filter-based estimators. The comparison is carried out using quantitative metrics such as estimation error, convergence behavior, and computational cost.

The main contributions of this work are summarized as follows:

- Development of a unified FMPC framework incorporating three nonlinear state estimators, namely the EKF, UKF, and PF, for fractional chaotic systems.

- Systematic comparison of the Extended Kalman Filter, Unscented Kalman Filter, and Particle Filter in terms of estimation accuracy, robustness, and computational efficiency.
- Analysis of partial-state observability scenarios and their impact on estimation performance in fractional-order dynamics.
- Demonstration of robust chaos stabilization and accurate state reconstruction under noisy measurement conditions.

The remainder of the paper is organized as follows. Section 2 introduces the Grünwald–Letnikov fractional derivative and its numerical implementation. Section 3 presents the fractional-order Rössler oscillator model and its dynamical properties. Section 4 details the FMPC formulation and the integration of nonlinear state estimators, including EKF, UKF, and PF. Section 5 provides a comprehensive comparative analysis of estimation and control performance under various noise conditions. Finally, Section 6 concludes the paper and outlines directions for future research.

2 Grüwald-Letnikov Fractional Derivative And Numerical Implementation

Fractional calculus generalizes classical integer-order differentiation to non-integer orders, providing a useful framework for modeling systems with memory effects and hereditary behavior. Unlike integer-order derivatives, which depend only on local information, fractional derivatives incorporate the past history of the state. This makes them suitable for representing long-range temporal dependencies in physical and engineering systems.

Among the various definitions of fractional derivatives, the Grünwald–Letnikov derivative, abbreviated as GL derivative, is particularly attractive for numerical implementation because it naturally leads to a discrete-time convolution form. In this work, D^{α}_{GL} denotes the Grünwald–Letnikov fractional derivative of order α. For a sufficiently smooth scalar function $f(t)$, evaluated at the discrete time instant $t_i = i\Delta t$, it is defined as [12, 21, 15]

$$D^{\alpha}_{GL} f(t_i) = \lim_{\Delta t \to 0} \frac{1}{\Delta t^{\alpha}} \sum_{n=0}^{i} (-1)^n \binom{\alpha}{n} f(t_i - n\Delta t), \tag{1}$$

where Δt is the time step and $\binom{\alpha}{n}$ denotes the generalized binomial coefficient defined by

$$\binom{\alpha}{n} = \frac{\Gamma(\alpha+1)}{\Gamma(n+1)\,\Gamma(\alpha-n+1)}, \tag{2}$$

with $\Gamma(\cdot)$ being the Gamma function.

For practical computations, the infinite-memory operator in (1) is approximated using a finite time step Δt and truncated memory length M, yielding

$$D^{\alpha}_{GL} f(t_i) \approx \frac{1}{\Delta t^{\alpha}} \sum_{n=0}^{M} (-1)^n \binom{\alpha}{n} f(t_{i-n}), \tag{3}$$

where $M \leq i$ represents the number of past samples retained in the computation. This truncation is commonly referred to as the *short-memory principle*, which significantly reduces computational cost while preserving the dominant memory effects [15, 21].

For clarity, Eq. (3) is first written for a scalar function $f(t)$. In the present work, the same operator is applied component-wise to the state vector of the dynamical system. Thus, for a state vector

$$X(t) = \begin{bmatrix} x(t) & y(t) & z(t) \end{bmatrix}^T,$$

the GL derivative is understood as

$$D^{\alpha}_{GL} X(t_k) = \begin{bmatrix} D^{\alpha}_{GL} x(t_k) \\ D^{\alpha}_{GL} y(t_k) \\ D^{\alpha}_{GL} z(t_k) \end{bmatrix}.$$

Therefore, the same coefficient sequence $\{w_n\}$ is used for each state component, and the memory term represents a weighted contribution of the past values of each state variable.

The coefficients $w_n = (-1)^n \binom{\alpha}{n}$ can be computed recursively as

$$w_0 = 1, \quad w_n = \left(1 - \frac{\alpha + 1}{n}\right) w_{n-1}, \quad n \geq 1, \tag{4}$$

which avoids repeated evaluation of Gamma functions and enhances numerical efficiency.

Using (3), the fractional derivative operator can be interpreted as a weighted convolution between the past states and the coefficient sequence $\{w_n\}$, thereby explicitly revealing the non-local and memory-dependent nature of the dynamics. This structure is particularly suitable for integration within predictive control frameworks, where past state information can be naturally incorporated into the prediction model.

For a general nonlinear fractional-order state-space system described by

$$D^{\alpha}_{GL} X(t) = F(X(t), u(t)), \tag{5}$$

where $X(t) \in \mathbb{R}^n$ is the state vector and $u(t)$ is the control input, the GL approximation leads to the discrete-time update

$$X_{k+1} = \Delta t^{\alpha} F(X_k, u_k) - \sum_{n=1}^{M} w_n X_{k+1-n}. \tag{6}$$

Equation (6) is applied component-wise. For the three-dimensional Rössler system, it gives separate update equations for x_{k+1}, y_{k+1}, and z_{k+1}, each containing its own finite-memory summation over the corresponding past state values.

In the numerical implementation, particular care is taken in the initialization of the GL memory history. For non-zero initial states, the past-history vector is initialized

consistently with the prescribed initial condition rather than being padded by zeros. This avoids introducing an artificial discontinuity at $t = 0$, which may otherwise create spurious initial transients in the fractional memory term. Such transients are numerical artifacts of the GL memory initialization and should not be interpreted as physical instability of the system.

The Grünwald–Letnikov formulation is therefore well suited for the present study, as it enables a direct and efficient incorporation of fractional dynamics into both the prediction model of the control scheme and the state estimation framework, while preserving the essential memory characteristics of the system.

3 Fractional-order Rössler Oscillator and Dynamical Properties

The fractional-order Rössler oscillator extends the classical integer-order system by incorporating non-local memory effects through fractional derivatives. Using the Grünwald–Letnikov (GL) formulation introduced in Section 2, the commensurate fractional-order Rössler system of order $\alpha \in (0, 1)$ is defined as

$$\begin{aligned} D^{\alpha}_{GL} x(t) &= -y(t) - z(t), \\ D^{\alpha}_{GL} y(t) &= x(t) + a\, y(t), \\ D^{\alpha}_{GL} z(t) &= b + z(t)\big(x(t) - c\big), \end{aligned} \tag{7}$$

where $x(t), y(t), z(t) \in \mathbb{R}$ are the state variables, and $a, b, c \in \mathbb{R}$ are system parameters [5, 6, 2, 1].

3.1 Discrete-Time Representation

For numerical implementation and integration within predictive control frameworks, the system (7) is discretized using the GL approximation derived in (6). Let $x_k = x(t_k)$ with $t_k = k\,\Delta t$, then the discrete-time fractional dynamics can be written as

$$\begin{aligned} x_{k+1} &= \Delta t^{\alpha}\big(-y_k - z_k\big) - \sum_{n=1}^{M} w_n x_{k+1-n}, \\ y_{k+1} &= \Delta t^{\alpha}\big(x_k + a\, y_k\big) - \sum_{n=1}^{M} w_n y_{k+1-n}, \\ z_{k+1} &= \Delta t^{\alpha}\big(b + z_k(x_k - c)\big) - \sum_{n=1}^{M} w_n z_{k+1-n}, \end{aligned} \tag{8}$$

where $\{w_n\}$ are the GL weights defined in (4). This formulation highlights the intrinsic non-Markovian nature of the system, as each state update depends on a finite history of past states.

3.2 Equilibrium Points

The equilibrium points of the fractional-order system are obtained by setting the right-hand side of (7) to zero. Since equilibrium conditions are independent of the derivative order, the fixed points coincide with those of the classical Rössler system. Solving

$$-y - z = 0, \quad x + ay = 0, \quad b + z(x - c) = 0,$$

yields two equilibrium points $f_p^{\pm} = (x^{\pm}, y^{\pm}, z^{\pm})$ given by

$$\begin{aligned} x^{\pm} &= \frac{c \pm \sqrt{c^2 - 4ab}}{2}, \\ y^{\pm} &= -\frac{x^{\pm}}{a}, \\ z^{\pm} &= \frac{x^{\pm}}{a}. \end{aligned} \tag{9}$$

3.3 Local Stability Analysis

To analyze the local stability of the system, we consider the Jacobian matrix of the vector field associated with (7), given by

$$J(x, y, z) = \begin{bmatrix} 0 & -1 & -1 \\ 1 & a & 0 \\ z & 0 & x - c \end{bmatrix}. \tag{10}$$

Evaluating (10) at the equilibrium points $f_p^{\pm}$ yields the linearized dynamics. For fractional-order systems of order $\alpha \in (0, 1)$, according to the Matignon criterion, local asymptotic stability requires that all eigenvalues λ_i of J satisfy the condition

$$|\arg(\lambda_i)| > \frac{\alpha\pi}{2}, \quad \forall i, \tag{11}$$

This condition reflects the sector stability region in the complex plane, which generalizes the classical requirement of negative real parts for integer-order systems [4, 22].

For the selected parameter set $a = 0.38$, $b = 4$, $c = 9$, and $\alpha = 0.9$, the equilibria are locally unstable. The eigenvalues of the Jacobian evaluated at f_p^{+} are approximately

$$\lambda_{1,2} = -0.0748 \pm 4.9207i, \qquad \lambda_3 = 0.3574,$$

while those at f_p^{-} are

$$\lambda_{1,2} = 0.1645 \pm 0.9794i, \qquad \lambda_3 = -8.7768.$$

The computed eigenvalues show that both equilibrium points are locally unstable according to Matignon's stability criterion, since at least one eigenvalue does not

satisfy the fractional-order stability condition $|\arg(\lambda_i)| > \alpha\pi/2$. This local instability indicates that the chosen parameter set is compatible with unstable oscillatory dynamics and motivates the use of control and state-estimation methods. However, local instability alone is not sufficient to prove chaos; the chaotic behavior is therefore further assessed through the simulated trajectories, phase portraits, and estimation/control performance presented in the following sections.

3.4 Dynamical Behavior

The fractional-order Rössler system exhibits a rich variety of dynamical behaviors, including periodic oscillations, quasi-periodicity, and chaos, depending on the system parameters and the fractional order α. The inclusion of fractional derivatives introduces additional degrees of freedom through memory effects, which influence transient responses, attractor geometry, and convergence properties.

In particular, changing the fractional order α modifies the memory contribution in the system and therefore changes the transient response, effective phase-space structure, and attractor geometry. Values of α close to unity recover dynamics similar to the classical integer-order Rössler system, whereas smaller values of α increase the relative influence of past states and may lead to more damped or qualitatively different responses depending on the parameter regime. The resulting chaotic trajectories are typically analyzed using phase portraits, time series, Lyapunov exponents, and error dynamics, providing a comprehensive characterization of system behavior prior to control design.

The complexity and sensitivity of these dynamics motivate the use of advanced control and estimation techniques, such as the FMPC and nonlinear state observers developed in this work.

4 Fractional Model Predictive Control with Nonlinear State Estimation

4.1 Fractional Model Predictive Control Formulation

Model Predictive Control (MPC) computes the control action by solving a finite-horizon optimization problem at each sampling instant [13, 28, 17, 18]. In the fractional-order case, the prediction model must account for the memory-dependent dynamics generated by the Grünwald–Letnikov approximation. The nonlinear fractional state-space model is written as

$$X_{k+1} = f_\alpha(X_k, u_k, \mathcal{H}_k) + W_k, \qquad Y_k = h(X_k) + V_k, \tag{12}$$

where

$$X_k = \begin{bmatrix} x_k \\ y_k \\ z_k \end{bmatrix} \in \mathbb{R}^3,$$

u_k is the control input, Y_k is the measured output, and

$$\mathcal{H}_k = \{X_{k-1}, X_{k-2}, \ldots, X_{k-M}\}$$

denotes the finite memory history used in the fractional approximation. The terms W_k and V_k represent process and measurement noise.

At each time instant k, the FMPC control action is obtained by solving the following finite-horizon constrained optimization problem:

$$\min_{\{u_{k+i|k}\}_{i=0}^{N_c-1}} \quad J_k = \sum_{i=0}^{N_p-1} \Big[\left(Y_{k+i|k} - r_{k+i}\right)^T Q \left(Y_{k+i|k} - r_{k+i}\right) + \Delta u_{k+i|k}^T R \Delta u_{k+i|k} \Big], \tag{13}$$

subject to

$$X_{k+i+1|k} = f_\alpha \left(X_{k+i|k}, u_{k+i|k}, \mathcal{H}_{k+i|k}\right), \tag{14}$$

$$u_{\min} \leq u_{k+i|k} \leq u_{\max}. \tag{15}$$

Here, N_p is the prediction horizon, N_c is the control horizon, $Y_{k+i|k} = h(X_{k+i|k})$ is the predicted output at future time $k+i$ computed at time k, and r_{k+i} is the corresponding reference trajectory. The matrix Q penalizes the output-tracking error, while R penalizes rapid variations of the control input. The control increment is defined as

$$\Delta u_{k+i|k} = u_{k+i|k} - u_{k+i-1|k}. \tag{16}$$

For $i = 0$, the previous input is the control value applied at the preceding sampling instant, i.e.,

$$u_{k-1|k} = u_{k-1}. \tag{17}$$

After solving the finite-horizon optimization problem, only the first element of the optimal control sequence is applied to the plant:

$$u_k = u_{k|k}^\star. \tag{18}$$

Since the complete state vector X_k is generally not available from measurements, the FMPC controller is initialized using an estimated state $\hat{X}_k$ obtained from a nonlinear observer. In this work, three observers are considered: the Extended Kalman Filter, the Unscented Kalman Filter, and the Particle Filter [11, 9, 25, 10].

4.2 Measurement Configurations

Two partial measurement cases are studied. In both cases, the measurement functions are linear selections of the full state vector. Therefore, the corresponding measurement matrices are equal to the Jacobians of the measurement functions with respect to the state vector.

In the first case, only the state z is measured:

$$Y_k = h_z(X_k) + V_k = z_k + V_k, \tag{19}$$

where

$$h_z(X_k) = \begin{bmatrix} 0 & 0 & 1 \end{bmatrix} X_k. \tag{20}$$

The corresponding measurement matrix is

$$H_z = \frac{\partial h_z}{\partial X} = \begin{bmatrix} 0 & 0 & 1 \end{bmatrix}. \tag{21}$$

In the second case, the states x and y are measured:

$$Y_k = h_{xy}(X_k) + V_k = \begin{bmatrix} x_k \\ y_k \end{bmatrix} + V_k, \tag{22}$$

where

$$h_{xy}(X_k) = \begin{bmatrix} 1 & 0 & 0 \\ 0 & 1 & 0 \end{bmatrix} X_k. \tag{23}$$

The corresponding measurement matrix is

$$H_{xy} = \frac{\partial h_{xy}}{\partial X} = \begin{bmatrix} 1 & 0 & 0 \\ 0 & 1 & 0 \end{bmatrix}. \tag{24}$$

4.3 Extended Kalman Filter

The Extended Kalman Filter (EKF) approximates the nonlinear fractional system by local linearization. The notation $\hat{X}_{k|k}$ denotes the estimate of the state at time k after using all measurements available up to time k. Similarly, $\hat{X}_{k+1|k}$ denotes the one-step-ahead prediction of the state at time $k+1$ using measurements available only up to time k [23, 26, 27]. Let

$$A_k = \left.\frac{\partial f_\alpha}{\partial X}\right|_{\hat{X}_{k|k}, u_k}, \qquad H_k = \left.\frac{\partial h}{\partial X}\right|_{\hat{X}_{k+1|k}}. \tag{25}$$

The EKF prediction step is given by

$$\hat{X}_{k+1|k} = f_\alpha\left(\hat{X}_{k|k}, u_k, \hat{\mathcal{H}}_k\right). \tag{26}$$

$$P_{k+1|k} = A_k P_{k|k} A_k^T + Q_p, \tag{27}$$

where $P_{k|k}$ is the estimation error covariance matrix associated with $\hat{X}_{k|k}$, and Q_p is the process-noise covariance matrix.

The predicted output and innovation are

$$\hat{Y}_{k+1|k} = h(\hat{X}_{k+1|k}), \tag{28}$$

$$r_{k+1} = Y_{k+1} - \hat{Y}_{k+1|k}. \tag{29}$$

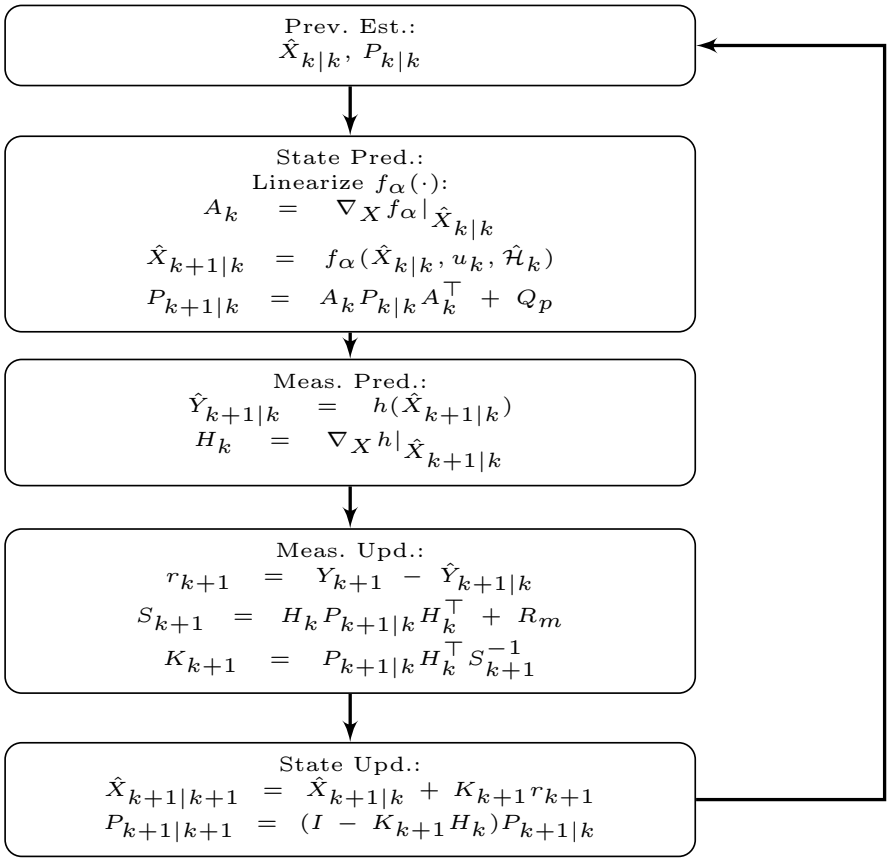


Fig. 1 Extended Kalman Filter implementation for fractional-order state estimation.

The innovation covariance and Kalman gain are

$$S_{k+1} = H_k P_{k+1|k} H_k^T + R_m, \tag{30}$$

$$K_{k+1} = P_{k+1|k} H_k^T S_{k+1}^{-1}, \tag{31}$$

where R_m is the measurement noise covariance.

The corrected state and covariance are then obtained as

$$\hat{X}_{k+1|k+1} = \hat{X}_{k+1|k} + K_{k+1} r_{k+1}, \tag{32}$$

$$P_{k+1|k+1} = (I - K_{k+1} H_k) P_{k+1|k}. \tag{33}$$

The EKF is computationally efficient because it propagates only one state estimate and one covariance matrix. However, its accuracy depends on the validity of the local linear approximation.

4.4 Unscented Kalman Filter

The Unscented Kalman Filter (UKF) is a nonlinear Gaussian state estimator. Unlike the EKF, it does not linearize the nonlinear model using Jacobian matrices. Instead, it approximates the propagation of uncertainty through the nonlinear dynamics by means of a deterministic set of sigma points.

The main assumption of the UKF is that, at each time instant, the conditional state distribution can be represented by a Gaussian approximation,

$$X_{k|k} \sim \mathcal{N}\left(\hat{X}_{k|k}, P_{k|k}\right), \tag{34}$$

where $\hat{X}_{k|k}$ is the estimated mean state and $P_{k|k}$ is the estimation error covariance matrix. Therefore, the complete probability density does not need to be stored explicitly. Instead, the filter only stores and propagates the mean and covariance of the state estimate.

From this Gaussian approximation, a finite set of deterministic sigma points is constructed. These sigma points are chosen so that their sample mean and covariance match $\hat{X}_{k|k}$ and $P_{k|k}$. After propagation through the nonlinear fractional model, the transformed sigma points are recombined to approximate the predicted mean and covariance.

The Unscented Kalman Filter (UKF) avoids explicit linearization by propagating deterministically selected sigma points through the nonlinear fractional model [11, 9]. For a state dimension n, define

$$\lambda = \rho^2(n + \kappa) - n, \tag{35}$$

where ρ and κ are scaling parameters.

The sigma points are generated as

$$\chi_k^{(0)} = \hat{X}_{k|k}, \tag{36}$$

$$\chi_k^{(i)} = \hat{X}_{k|k} + \left[\sqrt{(n+\lambda)P_{k|k}}\right]_i, \quad i = 1, \ldots, n, \tag{37}$$

$$\chi_k^{(i+n)} = \hat{X}_{k|k} - \left[\sqrt{(n+\lambda)P_{k|k}}\right]_i, \quad i = 1, \ldots, n. \tag{38}$$

The sigma points are not random particles. They are deterministically selected representative points of the Gaussian approximation $\mathcal{N}(\hat{X}_{k|k}, P_{k|k})$. These sigma points are propagated through the fractional dynamics:

$$\chi_{k+1|k}^{(i)} = f_\alpha(\chi_k^{(i)}, u_k, \mathcal{H}_k^{(i)}). \tag{39}$$

The predicted mean and covariance are

$$\hat{X}_{k+1|k} = \sum_{i=0}^{2n} W_i^m \chi_{k+1|k}^{(i)}, \tag{40}$$

$$P_{k+1|k} = \sum_{i=0}^{2n} W_i^c \left(\chi_{k+1|k}^{(i)} - \hat{X}_{k+1|k}\right) \left(\chi_{k+1|k}^{(i)} - \hat{X}_{k+1|k}\right)^T + Q_p. \tag{41}$$

Each predicted sigma point is then mapped through the measurement function:

$$\gamma_{k+1|k}^{(i)} = h(\chi_{k+1|k}^{(i)}). \tag{42}$$

The predicted measurement is

$$\hat{Y}_{k+1|k} = \sum_{i=0}^{2n} W_i^m \gamma_{k+1|k}^{(i)}. \tag{43}$$

The innovation covariance and cross-covariance are computed as

$$P_{yy} = \sum_{i=0}^{2n} W_i^c \left(\gamma_{k+1|k}^{(i)} - \hat{Y}_{k+1|k}\right) \left(\gamma_{k+1|k}^{(i)} - \hat{Y}_{k+1|k}\right)^T + R_m, \tag{44}$$

$$P_{xy} = \sum_{i=0}^{2n} W_i^c \left(\chi_{k+1|k}^{(i)} - \hat{X}_{k+1|k}\right) \left(\gamma_{k+1|k}^{(i)} - \hat{Y}_{k+1|k}\right)^T. \tag{45}$$

The UKF gain and correction step are

$$K_{k+1} = P_{xy} P_{yy}^{-1}, \tag{46}$$

$$\hat{X}_{k+1|k+1} = \hat{X}_{k+1|k} + K_{k+1} \left(Y_{k+1} - \hat{Y}_{k+1|k}\right), \tag{47}$$

$$P_{k+1|k+1} = P_{k+1|k} - K_{k+1} P_{yy} K_{k+1}^T. \tag{48}$$

The UKF is expected to provide improved estimation accuracy compared with the EKF in strongly nonlinear regions because it propagates nonlinear transformations more accurately without requiring Jacobian matrices.

4.5 Particle Filter

The Particle Filter (PF) is a sequential Monte Carlo state-estimation method that approximates the posterior probability density of the state by a finite cloud of random samples, called particles. Each particle represents one possible realization of the state trajectory, while its associated weight is a normalized importance weight that quantifies the relative credibility of that particle after the available measurement has been taken into account. In contrast to the EKF and UKF, the PF does not require the posterior distribution to be Gaussian and is therefore well suited for nonlinear and possibly non-Gaussian estimation problems.

At time instant k, the posterior density is numerically approximated by a finite set of weighted particles,

$$\left\{X_{k|k}^{(i)}, w_{k|k}^{(i)}\right\}_{i=1}^{N_s}, \tag{49}$$

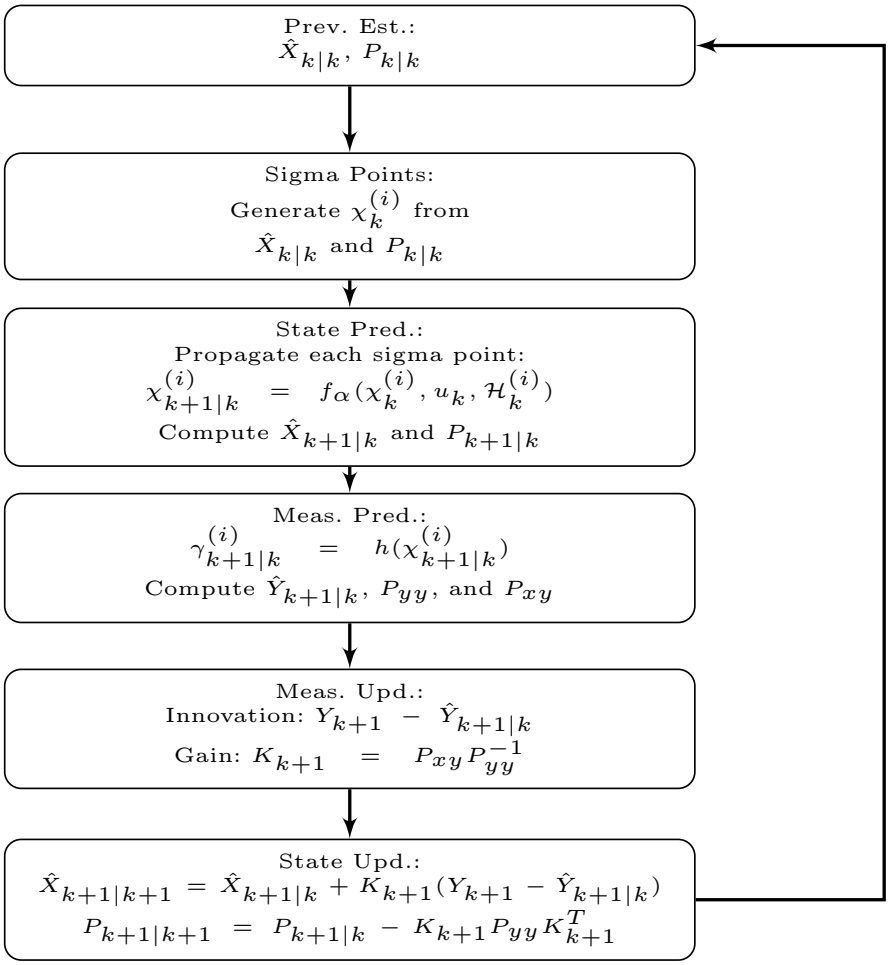


Fig. 2 Unscented Kalman Filter implementation for fractional-order state estimation.

where N_s is the number of particles. Each particle represents a possible state realization, while its normalized weight represents the relative contribution of that particle to the posterior approximation. The particles are then stochastically propagated through the process model by adding independent process-noise samples. The weights are normalized so that

$$\sum_{i=1}^{N_s} w_{k|k}^{(i)} = 1. \tag{50}$$

Each particle is first propagated through the nonlinear fractional model. Since the system is affected by process uncertainty, the propagation is performed stochastically as

$$X_{k+1|k}^{(i)} = f_\alpha\left(X_{k|k}^{(i)}, u_k, \mathcal{H}_k^{(i)}\right) + \eta_k^{(i)}, \tag{51}$$

where $\eta_k^{(i)}$ is a process-noise sample drawn for the ith particle. This step generates a predicted cloud of possible future states. The corresponding predicted measurement for each particle is then computed as

$$Y_{k+1|k}^{(i)} = h\left(X_{k+1|k}^{(i)}\right). \tag{52}$$

The weight update is based on the likelihood of the measured output Y_{k+1} given the predicted measurement of each particle. Assuming zero-mean Gaussian measurement noise with covariance matrix R_m, the likelihood of the ith particle is given by

$$L_{k+1}^{(i)} = \exp\left[-\frac{1}{2}\left(Y_{k+1} - Y_{k+1|k}^{(i)}\right)^T R_m^{-1}\left(Y_{k+1} - Y_{k+1|k}^{(i)}\right)\right]. \tag{53}$$

This expression corresponds to evaluating the Gaussian likelihood of the measurement prediction error $Y_{k+1} - Y_{k+1|k}^{(i)}$. Thus, the Gaussian assumption is made on the measurement noise, not on the particle weights themselves. The weights are normalized numerical coefficients obtained by evaluating this likelihood at each particle. Consequently, particles producing small prediction errors receive large likelihood values, whereas particles producing large prediction errors are exponentially penalized through the quadratic form involving R_m^{-1}. Through the weight update in Eq. (54), low-likelihood particles receive very small weights and are likely to be removed during resampling. Particles whose predicted measurements are close to the actual measurement receive larger likelihood values, whereas particles associated with large measurement errors receive small likelihood values.

The unnormalized weight of each particle is updated as

$$\widetilde{w}_{k+1}^{(i)} = w_{k|k}^{(i)} L_{k+1}^{(i)}, \tag{54}$$

and the weights are then normalized according to

$$w_{k+1|k+1}^{(i)} = \frac{\widetilde{w}_{k+1}^{(i)}}{\sum_{j=1}^{N_s} \widetilde{w}_{k+1}^{(j)}}. \tag{55}$$

This normalization ensures that the updated particle weights satisfy

$$\sum_{i=1}^{N_s} w_{k+1|k+1}^{(i)} = 1. \tag{56}$$

A common issue in particle filtering is particle degeneracy, where after A common issue in particle filtering is particle degeneracy, where after several iterations only a small number of particles carry most of the total weight. To detect this situation, the

effective sample size is evaluated as

$$N_{\text{eff}} = \frac{1}{\sum_{i=1}^{N_s} \left(w_{k+1|k+1}^{(i)} \right)^2}. \tag{57}$$

If N_{eff} falls below a prescribed threshold, resampling is performed. During resampling, particles with larger weights are statistically replicated, while particles with negligible weights are discarded. After resampling, the weights are typically reset to $1/N_s$. This step prevents the particle cloud from collapsing onto a few samples and preserves a representative approximation of the posterior distribution.

In practice, resampling alone may lead to sample impoverishment, because several copies of the same high-weight particles can be generated. In the present PF implementation, this effect is mitigated by the stochastic propagation step in Eq. (51): after resampling, the replicated particles are propagated with independent process-noise samples $\eta_k^{(i)}$. As a result, even particles originating from the same high-weight ancestor evolve differently at the next iteration, preserving diversity in the particle cloud.

Finally, the state estimate is computed as the weighted mean of the updated particle cloud:

$$\hat{X}_{k+1|k+1} = \sum_{i=1}^{N_s} w_{k+1|k+1}^{(i)} X_{k+1|k}^{(i)}. \tag{58}$$

The PF is therefore more flexible than the EKF and UKF because it directly approximates the posterior density using particles rather than imposing a linearized or Gaussian approximation. However, this flexibility comes at the cost of increased computational complexity, since a large number of particles may be required to obtain an accurate approximation of the posterior distribution.

4.6 Observer–FMPC Integration

The observer and FMPC are coupled in a receding-horizon structure. At each sampling instant, the available noisy measurement Y_k is processed by one of the nonlinear estimators to reconstruct the full state vector. The resulting estimate $\hat{X}_{k|k}$ initializes the FMPC prediction horizon.

The complete closed-loop procedure is summarized as follows:

1. Acquire the noisy partial measurement Y_k.
2. Estimate the full state $\hat{X}_{k|k}$ using EKF, UKF, or PF.
3. Use $\hat{X}_{k|k}$ and the fractional memory history $\hat{\mathcal{H}}_k$ to initialize the FMPC prediction model.
4. Solve the optimization problem (13).
5. Apply only the first optimal input $u_k = u_{k|k}^{\star}$.
6. Update the memory history and repeat the procedure at the next sampling instant.

This structure allows a direct and fair comparison of the three nonlinear estimators under the same FMPC law. The comparison is carried out in terms of estimation accuracy, robustness under measurement noise, convergence behavior, and computational cost.

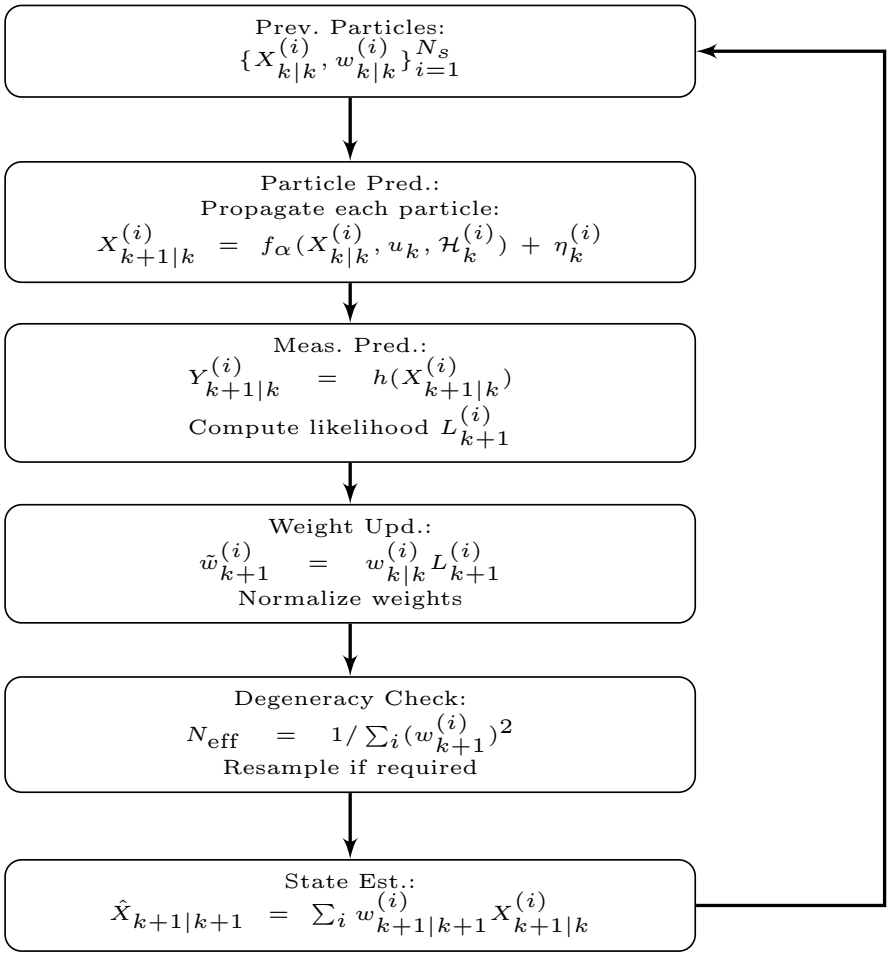


Fig. 3 Particle Filter implementation for fractional-order state estimation. The particles represent possible state realizations, the likelihood evaluates the measurement consistency of each particle, and the normalized weights define their relative contribution to the state estimate. Resampling reduces particle degeneracy, while stochastic propagation helps preserve particle diversity.

5 Results and Analyses

5.1 Numerical Analysis Parameters and Rationale

The numerical analyses are performed for the fractional-order Rössler oscillator with the system parameters

$$a = 0.38, \qquad b = 4, \qquad c = 9, \qquad \alpha = 0.9. \tag{59}$$

These values are selected because they generate chaotic transient behavior while preserving a well-defined unstable equilibrium for the control objective. The fractional order $\alpha = 0.9$ is chosen to represent a strong memory effect while remaining close to

the classical integer-order Rössler dynamics. The sampling time is fixed as

$$T_s = 1, \tag{60}$$

and the simulation is carried out over 3000 time steps, which is sufficiently long to observe the transient chaotic evolution, observer convergence, and closed-loop stabilization.

The target equilibrium is computed from the analytical fixed point of the Rössler system. For the chosen parameter values, this gives

$$(x^*, y^*, z^*) = (0.172183, -0.453113, 0.453113). \tag{61}$$

As shown by the local stability analysis in Section 3, this equilibrium is unstable in open loop according to the Matignon criterion. Therefore, it provides a meaningful stabilization target for the fractional model predictive controller.

The prediction horizon and control horizon are selected as

$$N_p = 30, \qquad N_c = 10. \tag{62}$$

The prediction horizon provides enough future information for the controller to anticipate the nonlinear fractional dynamics, while the shorter control horizon reduces the optimization burden. The input matrix is chosen as

$$B = \begin{bmatrix} 1 \\ 1 \\ 0 \end{bmatrix}, \tag{63}$$

meaning that the control input acts directly on the x and y equations, while the z state is influenced indirectly through nonlinear coupling.

The model predictive control weighting matrices are

$$Q = \begin{bmatrix} 5000 & 0 & 0 \\ 0 & 5000 & 0 \\ 0 & 0 & 1000 \end{bmatrix}, \qquad R = 20. \tag{64}$$

The large weights on x and y emphasize accurate tracking of the directly controlled states, while the smaller but still significant weight on z maintains stabilization of the nonlinear state. The control penalty $R = 20$ prevents excessive control effort and avoids overly aggressive input variations.

The input constraints are imposed as

$$-1 \leq u_k \leq 1, \tag{65}$$

which represents actuator saturation and ensures that the optimized control signal remains physically bounded. The nonlinear optimization is solved using the sequential quadratic programming algorithm through `fmincon`, since the predictive model contains nonlinear and fractional-memory-dependent terms.

For observer comparison, the process-noise covariance is selected as

$$Q_{\text{obs}} = \text{diag}(0.1, 0.1, 0.1). \tag{66}$$

This value reflects moderate uncertainty in the model dynamics and gives the filters sufficient flexibility to correct prediction errors. For the case where x and y are measured and z is estimated, the measurement-noise covariance is

$$R_{xy} = \text{diag}(0.5, 0.5). \tag{67}$$

This represents noisy measurements of the accessible states x and y. For the case where only z is measured and x, y are estimated, the measurement-noise variance is

$$R_z = 0.1. \tag{68}$$

This allows the second scenario to evaluate a more difficult partial-observation problem, since only one state is available for measurement.

For the Unscented Kalman Filter, the sigma-point parameters are chosen as

$$\alpha_u = 10^{-3}, \qquad \beta_u = 2, \qquad \kappa_u = 0. \tag{69}$$

The small value of α_u keeps the sigma points close to the mean, $\beta_u = 2$ is appropriate for Gaussian uncertainty, and $\kappa_u = 0$ is a common neutral scaling choice. For the Particle Filter, the number of particles is set to

$$N_s = 500. \tag{70}$$

This value provides a practical compromise between estimation accuracy and computational cost. A larger particle set may improve posterior approximation but would significantly increase computation time.

Hence, these parameters are selected to provide a consistent comparison between the Extended Kalman Filter, Unscented Kalman Filter, and Particle Filter under the same fractional model predictive control framework. The chosen settings allow the study to compare estimation accuracy, robustness to noisy measurements, and computational cost for two partial-measurement configurations.

5.2 Observer Performance under Partial Measurements

Two measurement configurations are considered to evaluate the performance of the EKF, UKF, and PF observers. The first case assumes that only z is measured, while x and y must be reconstructed. The second case assumes that x and y are measured, while z must be estimated.

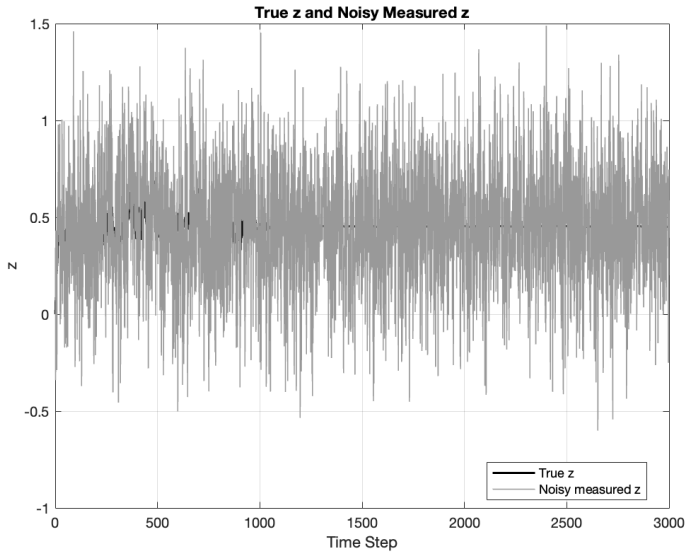


Fig. 4 True and noisy measured z signal for the z-only measurement case.

5.2.1 Case A: Only z Measured and x, y Estimated

This case represents the more difficult observer configuration because only the state z is available for measurement:

$$Y_k = z_k + v_k, \tag{71}$$

where v_k denotes zero-mean Gaussian measurement noise,

$$v_k \sim \mathcal{N}(0, R_z), \qquad R_z = 0.1. \tag{72}$$

Thus, the observers receive only a noisy scalar measurement of z and must reconstruct the unmeasured states x and y indirectly through the nonlinear coupling of the fractional Rössler dynamics.

Measured Output

From Fig. 4, the measured output follows the true z signal but is visibly corrupted by additive Gaussian noise. The fluctuations around the true trajectory are consistent with the measurement-noise variance $R_z = 0.1$ used in Eq. (72). Although the global trend of z remains visible, the measurement equation provides information only about the z component. Therefore, the reconstruction of x and y depends indirectly on the nonlinear coupling of the fractional Rössler dynamics, which makes accurate estimation more difficult.

Reconstruction of x and y

Figures 5 show the reconstruction performance of x and y. The EKF and UKF are able to loosely track the general trend of the true states but exhibit noticeable bias

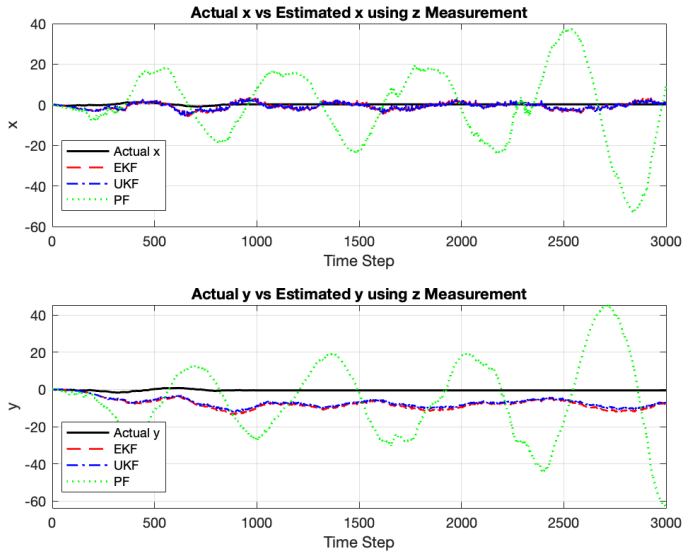


Fig. 5 Actual and estimated x and y using EKF, UKF, and PF when only z is measured.

and deviation. The estimation errors grow over time, especially for the y state, which shows larger amplitude mismatch. The Particle Filter performs significantly worse: its estimates diverge dramatically from the true trajectories, exhibiting large oscillations and instability. This indicates particle degeneracy and poor weight adaptation under insufficient measurement information.

Estimation Error

The absolute component-wise estimation errors $|e_x(k)|$ and $|e_y(k)|$ are useful for quantifying the reconstruction difficulty of the unmeasured states in the z-only measurement case. Since z is directly measured in this configuration, $|e_z(k)|$ mainly reflects the measurement noise level and the filtering effect of each observer. For each state component, the estimation error is defined as the pointwise absolute difference between the true state and its estimate:

$$e_x(k) = x_k - \hat{x}_k, \qquad e_y(k) = y_k - \hat{y}_k, \qquad e_z(k) = z_k - \hat{z}_k. \tag{73}$$

The quantities plotted in Fig. 6 correspond to the absolute component-wise errors,

$$|e_x(k)| = |x_k - \hat{x}_k|, \qquad |e_y(k)| = |y_k - \hat{y}_k|, \qquad |e_z(k)| = |z_k - \hat{z}_k|. \tag{74}$$

Thus, these are scalar absolute errors for each state component, not a vector norm of the full estimation error.

The error plots in Fig. 6 further highlight these observations. The EKF and UKF maintain bounded errors, although the magnitude is non-negligible, especially for y. In contrast, the PF exhibits extremely large error spikes, particularly at later time

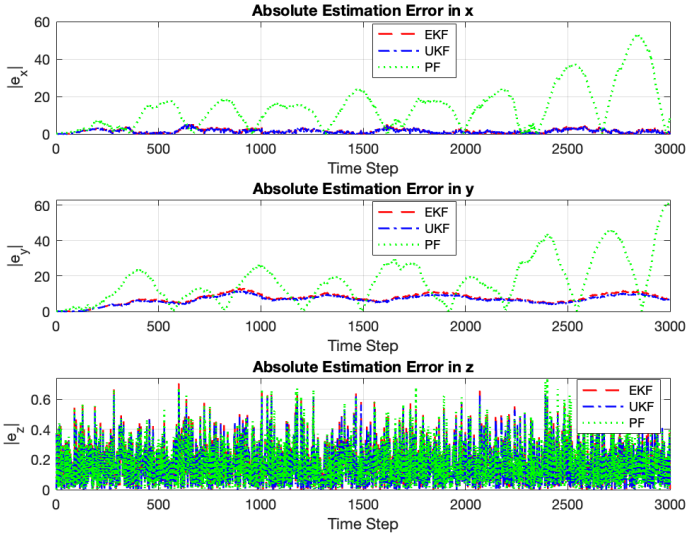


Fig. 6 Absolute component-wise estimation errors $|e_x(k)|$, $|e_y(k)|$, and $|e_z(k)|$ for the z-only measurement case.

steps, confirming its instability in this configuration. The error growth is consistent with the lack of sufficient observability when only one state is measured.

Quantitative Performance Comparison

The RMSE comparison in Fig. 7 clearly summarizes the estimation performance. The RMSE comparison in Fig. 7 summarizes the estimation performance for the z-only measurement case. The EKF and UKF achieve comparable reconstruction accuracy, with the UKF providing a slight improvement in this configuration. This improvement can be attributed to the sigma-point approximation used by the UKF, which propagates the mean and covariance through the nonlinear fractional dynamics without requiring an explicit first-order Jacobian linearization. However, both methods show larger errors for the unmeasured states, especially for y, confirming that reconstructing x and y from a single noisy measurement of z is difficult. The PF gives significantly larger RMSE values for both x and y, indicating poor performance under the selected number of particles and noise configuration. It should be emphasized that the EKF is also applicable to nonlinear systems; the difference is that it represents the local effect of the nonlinear dynamics through Jacobian-based linearization, whereas the UKF uses deterministic sigma points to approximate the propagation of uncertainty.

Computational Cost Analysis

Figure 8 compares the computational cost of the observers. The EKF is the fastest due to its linearization-based structure, followed by the UKF, which incurs additional cost from sigma point propagation. The PF is significantly slower due to the large number of particles and resampling operations. Despite its higher computational cost,

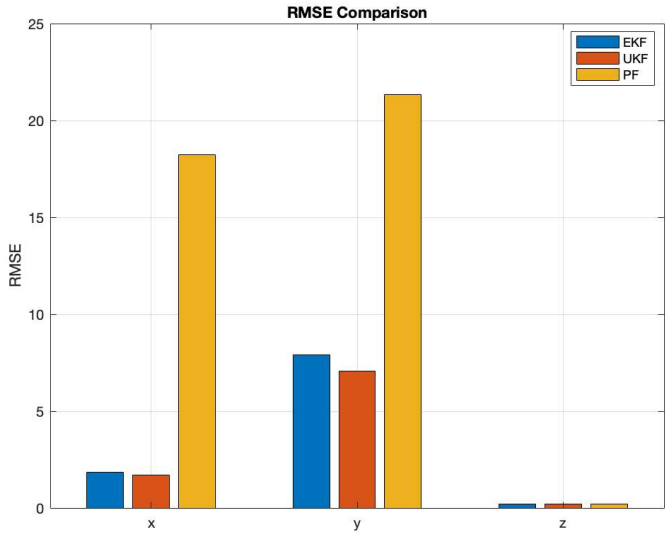


Fig. 7 RMSE comparison of EKF, UKF, and PF for the z-only measurement case.

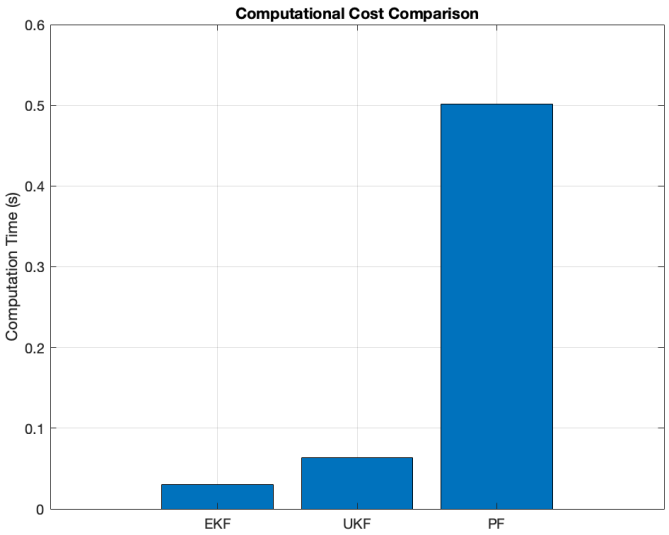


Fig. 8 Computational cost comparison of EKF, UKF, and PF the z measurement case.

the PF does not provide improved accuracy in this case, making it inefficient for this single-output reconstruction problem.

Discussion

The results demonstrate that when only z is measured, the system exhibits weak observability with respect to x and y. While EKF and UKF provide partially acceptable estimates, their accuracy remains limited. The PF fails to provide reliable estimates despite its computational complexity. These findings show that, for the considered fractional Rössler system, a single noisy measurement of z does not provide sufficient practical information to accurately reconstruct the unmeasured states x and y. This difficulty is amplified by the nonlinear coupling and memory-dependent fractional dynamics. In the z-only measurement configuration, the observer performance is significantly degraded due to weak observability of the system. The estimation errors for the unmeasured states x and y are large for all observers, with RMSE values reaching 1.86 and 7.89 for EKF, and 1.69 and 7.05 for UKF, respectively. Although the UKF slightly outperforms the EKF due to its better handling of nonlinearities, both filters fail to accurately reconstruct the hidden states. The Particle Filter exhibits the worst performance, with extremely large RMSE values (18.24 for x and 21.35 for y), indicating particle degeneracy and poor convergence under limited measurement information. Interestingly, the estimation of z itself remains relatively accurate across all methods, since it is directly measured. These results clearly demonstrate that relying on a single output severely limits the observer's ability to reconstruct the full system state, highlighting a fundamental observability limitation. This behavior can be interpreted from an observability perspective, as the measurement of a single nonlinear state does not provide sufficient information to reconstruct the full state vector, especially in the presence of noise and fractional memory effects.

5.2.2 Case B: x, y Measured and z Estimated

This case represents a more favorable observer configuration because two states are directly measured:

$$Y_k = \begin{bmatrix} x_k \\ y_k \end{bmatrix} + v_k. \tag{75}$$

The objective is to reconstruct the unmeasured nonlinear state z.

Measured Outputs

Figure 9 shows the true and noisy measurements of x and y. These two measured states provide richer information for the observer than the single-output z-only case.

Although the measurements are corrupted by significant additive noise, the measured channels still provide direct information about the states x and y. In Fig. 9, the true trajectories are plotted with thicker lines and superimposed on the noisy measurements to make the underlying signals visible. Compared with the z-only case, this measurement configuration provides richer information for reconstructing the unmeasured state z. In particular, the transient oscillatory behavior and convergence towards steady-state values can be identified. The presence of two measured states provides redundant and complementary information, which enhances the robustness of the estimation process despite measurement noise.

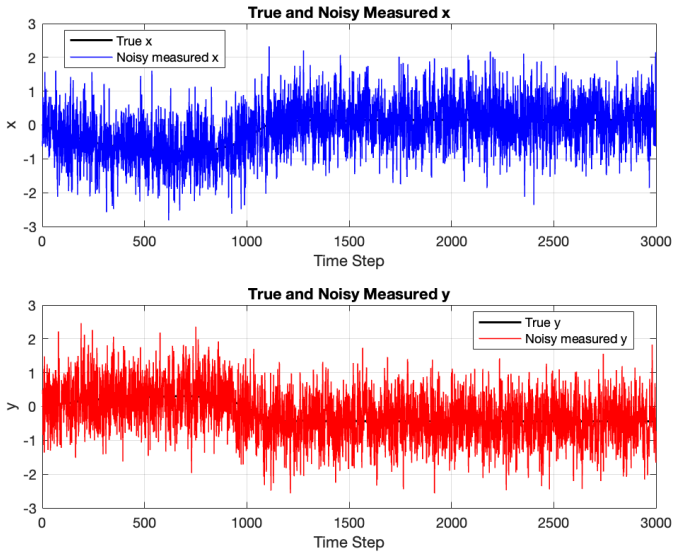


Fig. 9 True and noisy measured x and y signals for the x, y measurement case.

Reconstruction of z

Figure 10 presents the reconstruction of the unmeasured state z. The EKF and UKF show excellent tracking performance, with estimated trajectories almost overlapping the true z signal throughout the entire time horizon. This demonstrates that the nonlinear coupling between (x, y) and z is sufficiently informative for accurate reconstruction. In contrast, the Particle Filter exhibits larger fluctuations and noise in its estimates, although it still captures the general trend of the z dynamics. This behavior is consistent with the stochastic nature of particle-based methods.

Estimation Error

The absolute error $|e_z|$ highlights the reconstruction accuracy of the unmeasured state.

The absolute error plot in Fig. 11 shows that the EKF and UKF maintain very low estimation error for z, with small fluctuations around zero. The error remains bounded and does not exhibit divergence over time. In contrast, the PF shows significantly higher error variance, with occasional spikes indicating estimation uncertainty. However, even in this case, the error remains within acceptable limits compared to Case A.

Quantitative Performance Comparison

The RMSE and MAE comparisons in Figs. 12 and 13 confirm the qualitative observations. The EKF and UKF achieve nearly identical performance, with very low error values for z, demonstrating their effectiveness in nonlinear estimation with sufficient measurements. The PF shows a noticeably higher RMSE and MAE for z, reflecting

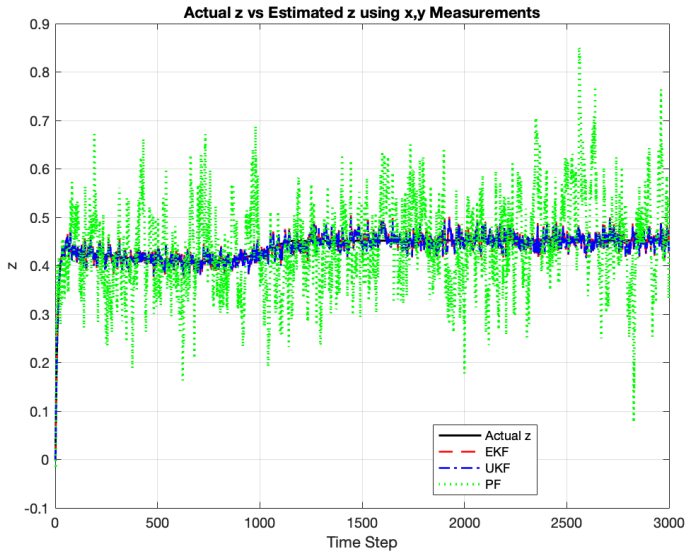


Fig. 10 Actual and estimated z using EKF, UKF, and PF when x and y are measured.

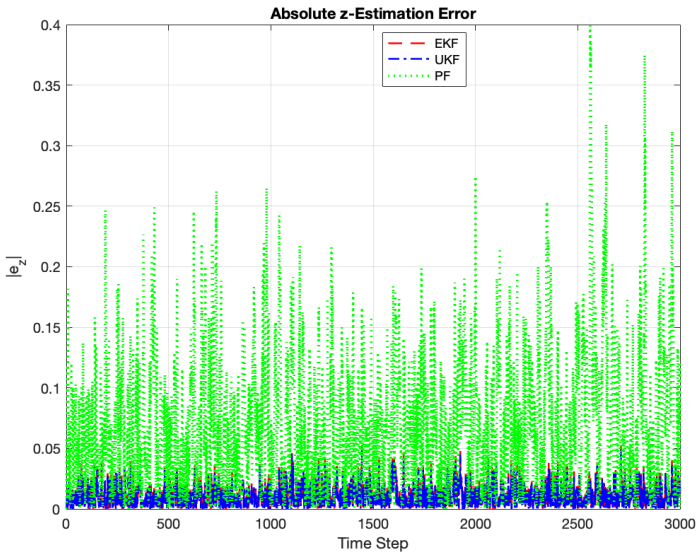


Fig. 11 Absolute estimation error $|e_z|$ for the x, y measurement case.

its sensitivity to noise and sampling variability. For the measured states x and y, all methods yield similar error values since these states are directly observed.

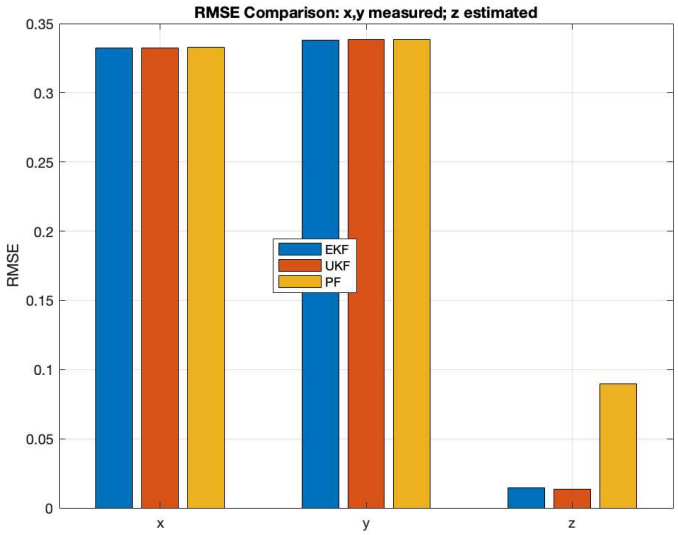


Fig. 12 RMSE comparison of EKF, UKF, and PF for the x, y measurement case.

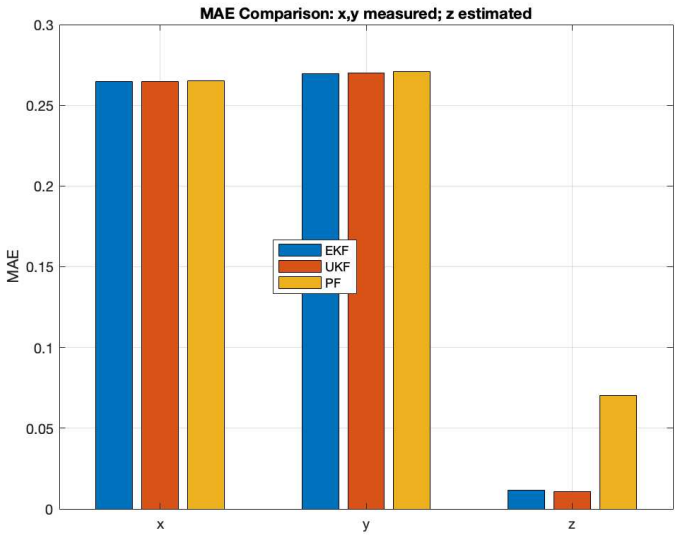


Fig. 13 MAE comparison of EKF, UKF, and PF for the x, y measurement case.

5.2.3 Computational Cost Comparison

In addition to estimation accuracy, computational time is compared because observer selection is important for real-time fractional model predictive control.

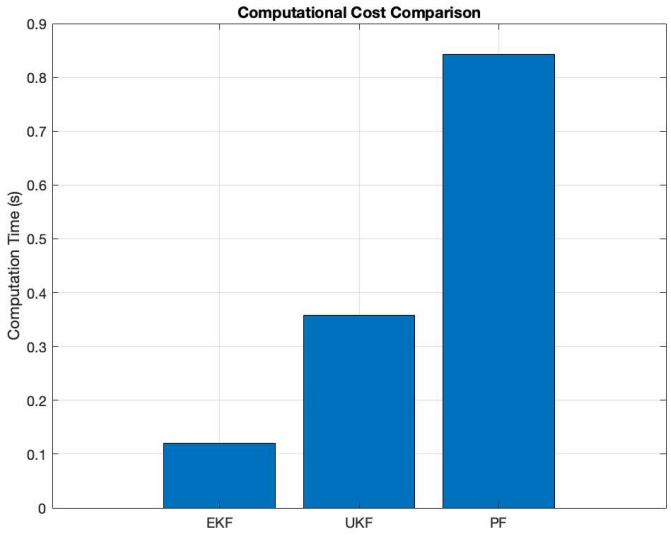


Fig. 14 Computational cost comparison of EKF, UKF, and PF for the x, y measurement case.

Figure 14 compares the computational time of the three observers. The EKF remains the most computationally efficient method, with an average computation time of approximately 0.13 s. The UKF requires approximately 0.39 s, which is about three times higher than the EKF, mainly due to the propagation of sigma points. The PF requires approximately 0.80 s, corresponding to about six times the EKF computation time and about two times the UKF computation time. This additional cost is caused by particle propagation, likelihood evaluation, weight normalization, and resampling. Despite this increased computational burden, the PF does not provide superior estimation accuracy in this configuration, making it less suitable for real-time implementation under the selected particle size.

Discussion

The results clearly demonstrate that measuring x and y significantly improves the observability of the system and enables accurate reconstruction of the unmeasured state z. The EKF and UKF achieve near-optimal performance with low estimation error and high robustness to noise. The PF, although capable of capturing the general dynamics, suffers from higher variance and a substantially larger computational cost: in the present case, its average computation time is approximately 0.80 s, compared with 0.13 s for the EKF and 0.39 s for the UKF. These findings highlight the importance of sensor configuration in observer design and confirm that multi-state measurements are critical for reliable estimation in fractional-order nonlinear systems. When both x and y are measured, the observer performance improves dramatically, and the unmeasured state z can be accurately reconstructed. Both EKF and UKF achieve very low estimation errors for z (RMSE $\approx$ 0.0146 and 0.0136, respectively),

indicating near-perfect tracking. The PF also estimates z reasonably well, but with noticeably higher error and approximately 6.2 times the computational cost of the EKF. The RMSE and MAE values for x and y are similar across all methods, as these states are directly measured with noise. Overall, the UKF provides the best estimation accuracy, while the EKF offers a favorable trade-off between accuracy and computational efficiency. These findings further confirm that the availability of multiple measured states improves practical state reconstruction and enables reliable estimation of the remaining state through nonlinear coupling in the Rössler dynamics.

5.2.4 Discussion

The z-only measurement case is more challenging because the observers must infer two unmeasured states from a single noisy output. As a result, the reconstruction errors for x and y are significantly larger. In contrast, when x and y are measured, the unmeasured state z can be reconstructed more accurately due to stronger dynamic coupling and richer measurement information. Overall, the UKF provides the best estimation accuracy, while the EKF offers the most favorable trade-off between accuracy and computational cost. The PF requires higher computational effort and shows weaker performance under the selected number of particles.

6 Conclusion and Future Scope

This paper presented a comparative observer-FMPC framework for the fractional-order Rössler chaotic system. The fractional dynamics were modeled using the Grünwald–Letnikov approximation, allowing memory effects to be incorporated into the predictive control formulation. Three nonlinear observers, namely the Extended Kalman Filter, Unscented Kalman Filter, and Particle Filter, were evaluated under partial measurement conditions. Two partial measurement configurations were considered: (i) only z measured, with x and y reconstructed by the observer, and (ii) x and y measured, with z reconstructed by the observer.

The numerical results show that the measurement configuration has a strong influence on estimation performance. When only z is measured, reconstruction of x and y becomes difficult, indicating weak practical state reconstruction under this sensor configuration. In this case, the UKF provides slightly better accuracy than the EKF, while the PF exhibits larger estimation errors and higher computational cost. In contrast, when x and y are measured, the unmeasured state z is reconstructed accurately. The EKF and UKF achieve very low estimation errors, with the UKF giving the best accuracy and the EKF offering the most favorable balance between estimation performance and computation time. The PF remains computationally expensive and less accurate under the selected particle size. Overall, the results show that observer selection and sensor configuration are critical for reliable state reconstruction and control of fractional-order chaotic systems.

Future work will focus on strengthening both the theoretical and practical aspects of the proposed framework. First, a rigorous stability analysis of the closed-loop FMPC–observer system can be developed using fractional Lyapunov theory to establish boundedness and convergence of the estimation and control errors. Second, the

observer framework can be extended by including fractional Kalman filters and other nonlinear estimators, with a deeper comparison of accuracy, robustness, and computational cost. Third, the proposed method can be generalized to other fractional chaotic systems, such as Lorenz, Duffing, and Chua oscillators, to demonstrate that the framework is not limited to the Rössler system.

A more comprehensive robustness study can also be performed under parameter uncertainty, impulsive noise, sensor faults, and measurement delays. Additional extensions may include bifurcation and Lyapunov exponent analysis to quantify chaos suppression, computational complexity analysis for real-time feasibility, and learning-based tuning of MPC parameters using neural networks or reinforcement learning. These directions would improve the theoretical depth, generality, and practical relevance of the proposed observer-based FMPC framework.

Declarations

- **Funding**
  Funding information – not applicable.
- **Conflict of interest/Competing interests**
  The authors declare that they have no competing interests.
- **Ethics approval and consent to participate**
  Not applicable. This study does not involve human participants, human data, or animals.
- **Consent for publication**
  Not applicable.
- **Data availability**
  The data used in this study were generated through numerical simulations of the fractional-order Rössler system and the associated observer–FMPC framework. No external experimental datasets were used. The simulation parameters required to reproduce the results are provided in the manuscript. Additional numerical data are available from the corresponding author upon reasonable request.
- **Materials availability**
  Not applicable.
- **Code availability**
  The simulation codes used to generate the numerical results are available from the corresponding author upon reasonable request.

References

[1] A.I. Ahmed et al. “Chaos and Bifurcations in the Dynamics of the Variable-Order Fractional Rössler System”. In: *Mathematics* 13.22 (2025), p. 3695.

[2] R. Allogmany and S. S. Alzahrani. “Dynamic, Bifurcation, and Lyapunov Analysis of Fractional Rössler Chaos Using Two Numerical Methods”. In: *Mathematics* 13.22 (2025), p. 3642.

[3] D. Boudjehem and B. Boudjehem. “A fractional model predictive control for fractional order systems”. In: *Fractional Dynamics and Control*. Springer, 2011, pp. 59–71.

[4] J. Čermák and L. Nechvátal. “Local bifurcations and chaos in the fractional Rössler system”. In: *International Journal of Bifurcation and Chaos* 28.08 (2018), p. 1850098.
[5] D. Das, I. Taralova, and J.-J. Loiseau. “Time-delay feedback control of fractional chaotic Rössler oscillator”. In: *IFAC-PapersOnLine* 58.5 (2024), pp. 90–95.
[6] D. Das et al. “Fractional model predictive control of fractional chaotic Rössler oscillator”. In: *IFAC-PapersOnLine* 59.11 (2025), pp. 156–161.
[7] D. Das et al. “Fractional-Order Coupled Oscillators for Synchronization-Based Gait Control in Hexapod Robots”. In: *Proceedings of the 18th CHAOS 2025 International Conference (CHAOS 2025)*. In Press. Athens, Greece, 2025.
[8] D. Das et al. “State Estimation using Extended Kalman Filter for Fractional Model Predictive Control of Fractional Chaotic Rössler Oscillator”. In: *Proceedings of the 11th International Conference on Control, Decision and Information Technologies (CoDIT)*. IEEE, 2025, pp. 1530–1535.
[9] K. György, A. Kelemen, and L. Dávid. “Unscented Kalman filters and particle filter methods for nonlinear state estimation”. In: *Procedia Technology* 12 (2014), pp. 65–74.
[10] T. Jiang, J. Chen, and Y. Wang. “A novel fractional nonlinear state estimation algorithm in non-Gaussian noise”. In: *Measurement* 227 (2024), p. 114261.
[11] S. Konatowski, P. Kaniewski, and J. Matuszewski. “Comparison of estimation accuracy of EKF, UKF and PF filters”. In: *Annual of Navigation* 23 (2016), pp. 69–87.
[12] J. L. Lavoie, J. T. Osler, and R. Tremblay. “Fractional derivatives and special functions”. In: *SIAM Review* 18.2 (1976), pp. 240–268.
[13] J. M. Maciejowski, P. J. Goulart, and E. C. Kerrigan. “Constrained control using model predictive control”. In: *Advanced Strategies in Control Systems with Input and Output Constraints*. Berlin: Springer, 2007, pp. 273–291.
[14] E. C. de Oliveira and J. A. Tenreiro Machado. “A review of definitions for fractional derivatives and integrals”. In: *Mathematical Problems in Engineering* (2014).
[15] M. K. Owolabi and A. Atangana. *Numerical Methods for Fractional Differentiation*. Vol. 54. Singapore: Springer, 2019.
[16] I. Petráš. “Fractional-order chaotic systems”. In: *Fractional-order Nonlinear Systems: Modeling, Analysis and Simulation*. Berlin, Heidelberg: Springer, 2021, pp. 103–184.
[17] I. Petráš. “Novel fractional-order model predictive control: State-space approach”. In: *IEEE Access* 9 (2021), pp. 92769–92775.
[18] A. Rhouma and F. Bouani. “Robust model predictive control of uncertain fractional systems: a thermal application”. In: *IET Control Theory & Applications* 8.17 (2014), pp. 1986–1994.
[19] M. Romero et al. “A survey of fractional-order generalized predictive control”. In: *Proceedings of the 51st IEEE Conference on Decision and Control*. 2012, pp. 6867–6872.
[20] O. E. Rössler. “An equation for continuous chaos”. In: *Physics Letters A* 57.5 (1976), pp. 397–398.

[21] R. Scherer et al. “The Grünwald–Letnikov method for fractional differential equations”. In: *Computers and Mathematics with Applications* 62.3 (2011), pp. 902–917.

[22] N. Sene. “Analysis of a fractional-order chaotic system in the context of the Caputo fractional derivative via bifurcation and Lyapunov exponents”. In: *Journal of King Saud University - Science* 33.1 (2021), p. 101275.

[23] D. Sierociuk and A. Dzielinski. “Fractional Kalman filter algorithm for the states, parameters and order of fractional system estimation”. In: *International Journal of Applied Mathematics and Computer Science* 16.1 (2006), pp. 129–140.

[24] D. Song et al. “An adaptive fractional-order extended Kalman filtering approach for estimating state of charge of lithium-ion batteries”. In: *Journal of Energy Storage* 85 (2024), p. 111089.

[25] G. Wang and X. Sun. “Robust Kalman filter for fractional order systems with uncertain colored noise variance”. In: *Measurement and Control* 57.10 (2024), pp. 1445–1455.

[26] C. Yang et al. “Adaptive fractional-order Kalman filters for continuous-time nonlinear fractional-order systems with unknown parameters and fractional-orders”. In: *International Journal of Systems Science* 52.13 (2021), pp. 2777–2797.

[27] W. Yu et al. “A fractional high-order extended kalman filter for fractional-order nonlinear systems”. In: *ISA Transactions* (2026).

[28] A. Zenere and M. Zorzi. “Model predictive control meets robust Kalman filtering”. In: *IFAC-PapersOnLine* 50.1 (2017), pp. 3774–3779.